



Modeling the sharp compositional interface in the Pu'u'Ō'ō magma reservoir, Kīlauea volcano, Hawai'i

Eric Mittelstaedt and Michael O. Garcia

Department of Geology and Geophysics, University of Hawai'i, 1680 East-West Road, Honolulu, Hawaii 96822, USA
(staggles@soest.hawaii.edu)

[1] Lavas from the early episodes of the Pu'u'Ō'ō eruption (1983–1985) of Kīlauea Volcano on the island of Hawai'i display rapid compositional variation over short periods for some episodes, especially the well-sampled episode 30 with ~2 wt% MgO variation in <4 hours. Little chemical variation is observed within the episode 30 lavas before or after this abrupt change, suggesting a sharp compositional interface within the Pu'u'Ō'ō dike-like shallow reservoir. Cooling-induced crystal fractionation in this reservoir is thought to be the main control on intraepisode compositional variation. Potential explanations for a sharp interface, such as changing reservoir width and wall rock thermal properties, are evaluated using a simple thermal model of a dike-like body surrounded by wall rock with spatially variable thermal conductivity. The model that best reproduces the compositional data involves a change in wall rock thermal conductivity from 2.7 to 9 W m⁻¹ C⁻¹, which is consistent with deep drill hole data in the east rift zone. The change in thermal conductivity may indicate that fluid flow in the east rift zone is restricted to shallow depths possibly by increasing numbers of dikes acting as aquicludes and/or decreasing pore space due to formation of secondary minerals. Results suggest that wall rock thermal gradients can strongly influence magma chemistry in shallow reservoirs.

Components: 7035 words, 11 figures, 2 tables.

Keywords: numerical modeling; magma reservoir; Kīlauea; Hawai'i.

Index Terms: 1036 Geochemistry: Magma chamber processes (3618); 8145 Tectonophysics: Physics of magma and magma bodies; 3037 Marine Geology and Geophysics: Oceanic hotspots and intraplate volcanism.

Received 27 October 2006; **Revised** 16 February 2007; **Accepted** 28 February 2007; **Published** 25 May 2007.

Mittelstaedt, E., and M. O. Garcia (2007), Modeling the sharp compositional interface in the Pu'u'Ō'ō magma reservoir, Kīlauea volcano, Hawai'i, *Geochem. Geophys. Geosyst.*, 8, Q05011, doi:10.1029/2006GC001519.

1. Introduction

[2] Kīlauea, on the island of Hawai'i (Figure 1), is one of the most active and best studied volcanoes in the world. The current eruption of Kīlauea started in 1983 and is continuing. It is one of the world's best monitored eruptions [Heliker and Mattox, 2003]. Field and geophysical data on Kīlauea are collected nearly continuously by the staff of the U.S. Geological Survey's Hawaiian

Volcano Observatory. In addition, previous field, petrologic, geochemical and geophysical studies have established the basic structure of the volcano's magmatic plumbing system [e.g., Ryan, 1988; Tilling and Dvorak, 1993; Pietruszka and Garcia, 1999]. Thus many of the basic parameters needed for modeling magma chamber processes are known for this eruption. Some of these parameters include magma temperatures, reservoir size and shape, effusion rates and geothermal gradients [Keller et

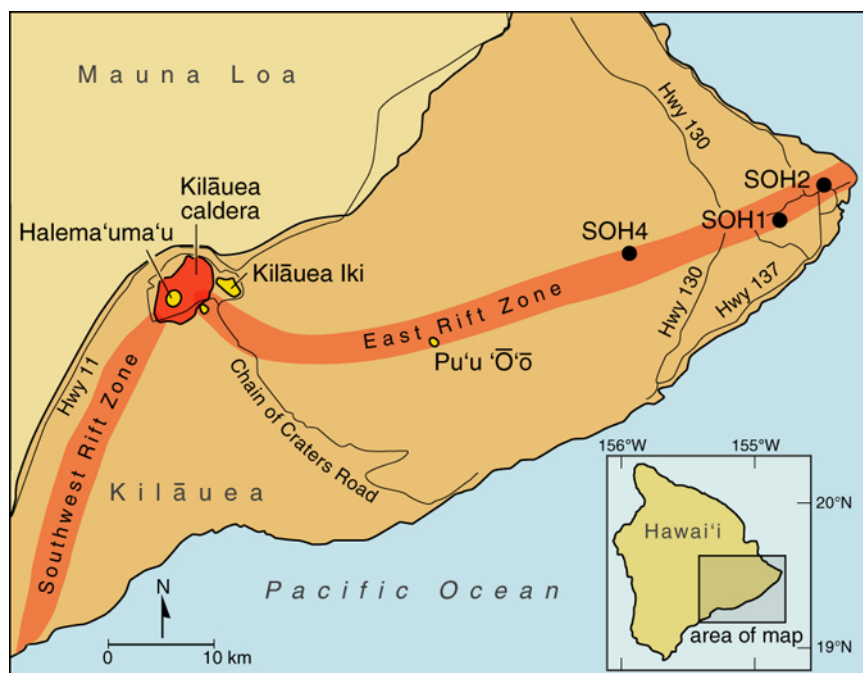


Figure 1. Pu`u`O`o is located within the east rift zone of Kīlauea volcano on the island of Hawai'i. Boreholes SOH 1, 2, and 4 (black dots) are locations of geothermal wells where measurements of the thermal gradient, stratigraphy, and fluid flow within the east rift zone were taken. Figure modified after *Bargar et al.* [1995].

al., 1979; *Wolfe et al.*, 1988; *Hoffmann et al.*, 1990; *Bargar et al.*, 1995]. The high frequency of its eruptions, their easy accessibility and the extensive database have made Kīlauea a superb location for modeling volcanic processes (e.g., degassing [*Vergnolle and Jaupart*, 1990], dike intrusion [*Parfitt and Wilson*, 1994; *Troise*, 2001], crustal structure [*Okubo et al.*, 1997]; summit magma chamber size and residence time [*Pietruszka and Garcia*, 1999]).

[3] Some of the early episodes of the Pu`u`O`o eruption (5–10, 30 and 31) during 1983–1985 are particularly interesting because they are characterized by significant compositional variation (up to 2 wt% MgO) in the erupted lava during these brief episodes (<4 days [*Garcia and Wolfe*, 1988; *Garcia et al.*, 1992]). Episode 30, the most frequently sampled of the compositionally variable episodes, displayed the majority of its compositional variation (~90%) during <4 hours suggesting that the Pu`u`O`o reservoir had a sharp compositional interface.

[4] Sharp compositional interfaces are documented for many magma chambers (e.g., Paricutin [*Wilcox*, 1954]). Typically, these interfaces separate magmas with striking compositional differences (silicic and mafic [*Koyaguchi*, 1989]) that result from magma mixing [*Kuritani et al.*, 2003]. In some cases,

however, sharp compositional gradients in solidified magma reservoirs are thought to be related to in situ crystal fractionation resulting from country rock thermal gradients (e.g., Shonkin Sag, Montana and Palisades sill, New Jersey [*Latypov*, 2003]). The Pu`u`O`o eruption presents an opportunity to test this and other hypotheses for creating compositional variation in magma reservoirs using a well-constrained situation. The Pu`u`O`o reservoir was partially to completely flushed during some eruptive episodes allowing a new batch of magma to recharge the reservoir [*Garcia et al.*, 1992; *Shamberger and Garcia*, 2007]. During the 8–36 days between eruptive episodes, this batch of homogeneous magma underwent cooling in a dike producing a chemically zoned magma reservoir with a sharp interface [*Garcia et al.*, 1992]. Potential processes for producing a sharp compositional interface in the shallow Pu`u`O`o magma reservoir are evaluated below using a simple cooling model, focusing on episode 30. The modeling results should be applicable to other reservoirs that display sharp compositional variations.

2. Geologic Setting and Eruption Summary

[5] A primary conduit extending from mantle depths of at least 60 km supplies magma to the

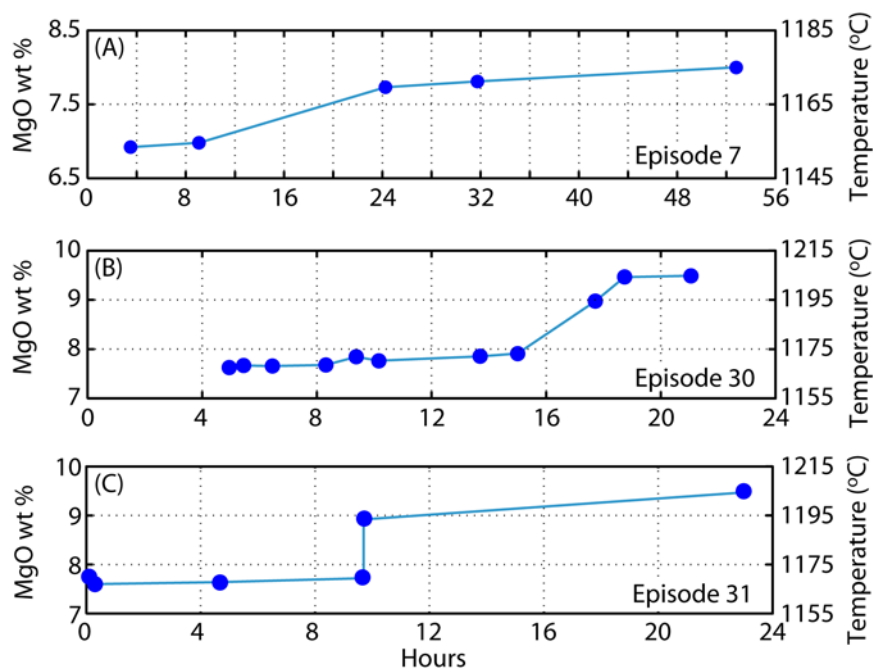


Figure 2. The temporal MgO variation during episodes (a) 7, (b) 30, and (c) 31 shows evidence for a sharp compositional boundary in the dike-like magma reservoir beneath the Pu`u`O`o vent. Data from *Garcia and Wolfe* [1988] and M. Garcia et al. (manuscript in preparation, 2007).

3–6 km deep summit reservoir at Kīlauea volcano [*Klein et al.*, 1987]. This reservoir and the primary mantle conduit feed magma to the rift zones that trend southwest and east of the summit at depths of 2–4 km [*Dzurisin et al.*, 1984; *Ryan*, 1988]. The east rift has been Kīlauea’s main region of effusive activity for the last 50 years [*Macdonald et al.*, 1983] including the ongoing Pu`u`O`o eruption, which began on 03 Jan 1983, ~15 km from the summit. The Pu`u`O`o eruption was triggered by a dike intrusion from the upper east rift zone [*Wolfe et al.*, 1987] during the current period of high magma supply (up to 0.18 km³/year [*Cayol et al.*, 2000]). Lavas from episode 1 of this eruption are hybrids resulting from mixing two rift zone-stored, differentiated magmas [*Garcia et al.*, 1989]. The composition of subsequent lavas (episodes 2–19) reflects mixing between this early hybrid magma and an MgO-rich new magma in the deep reservoir [*Shamberger and Garcia*, 2007]. By episode 20, no chemical or petrographic signs of mixing are evident and the erupted lavas are thought to consist entirely of the new magma. Separate from these inter-episodic variations, intraepisodic variations in MgO content (starting with lower MgO followed later by higher MgO lavas) indicate chemical zonation within the shallow magma reservoir resulting primarily from olivine fractionation

[*Garcia et al.*, 1992]. Intraepisodic MgO variation is largest for lavas from episodes 5–10, 30 and 31 (Figures 2 and 3).

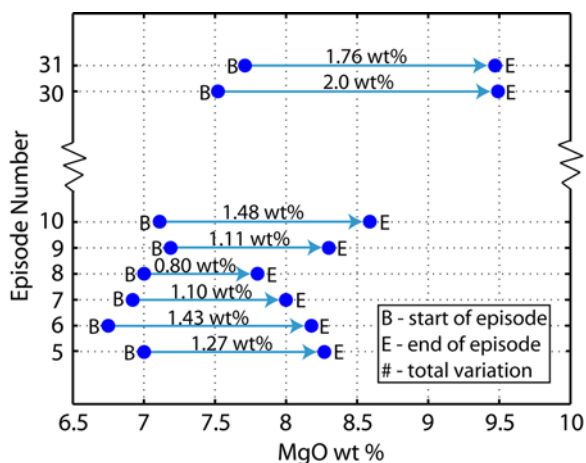


Figure 3. The MgO variation for episodes 5–10, 30, and 31 demonstrates the existence of a compositional boundary in Pu`u`O`o’s shallow magma reservoir prior to these episodes. Unfortunately, too few samples were taken during episodes 5–10 and 31 to quantitatively evaluate the nature of the variation. Data from *Garcia and Wolfe* [1988], *Garcia et al.* [1992], and M. Garcia et al. (manuscript in preparation, 2007).

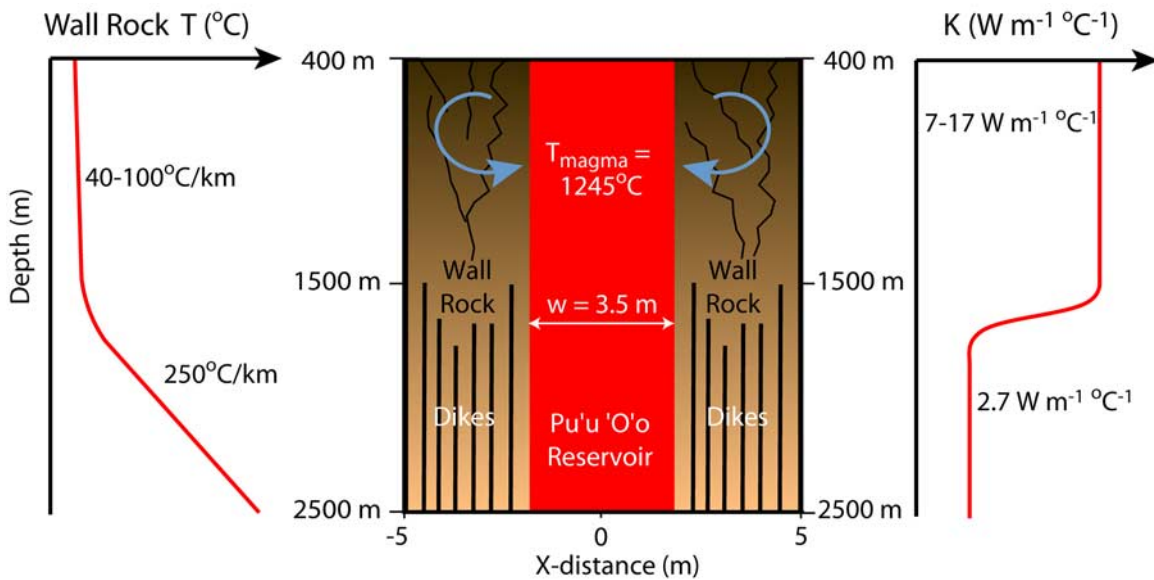


Figure 4. The conceptual model of the dike reservoir beneath the Pu'u 'Ō'Ō vent. The geotherm in 3 boreholes (SOH1, SOH2, and SOH4) along Kīlauea's east rift zone changes from $\sim 40\text{--}100^\circ\text{C}/\text{km}$ to $\sim 250^\circ\text{C}/\text{km}$ between 1650 m and 1950 m [Bargar *et al.*, 1995]. This change in thermal gradient may be related to enhanced groundwater circulation (blue arrows) in a shallow fractured (jagged black lines) section and poor circulation in the lower section where dikes (vertical black lines) are more common [Macdonald *et al.*, 1983; Quane *et al.*, 2000]. This variation in groundwater circulation is probably responsible for a greater thermal conductivity at shallow depths.

[6] The geometry and size of the shallow Pu'u 'Ō'Ō magma reservoir were evaluated on the basis of surface deformation studies conducted during episodes 22–42. Modeling of these results indicated that the reservoir was a narrow, vertical, ~ 3.5 m wide, ~ 1.6 km long and ~ 3 km deep dike with a top at a depth of ~ 0.4 km [Okamura *et al.*, 1988; Hoffmann *et al.*, 1990]. The dike volume is thought to have increased from ~ 3 Mm³ initially to at least 10–12 Mm³ by episode 10 [Hoffmann *et al.*, 1990]. This shallow reservoir overlies a larger reservoir (46–49 Mm³) within the core of the rift zone which is the site of magma mixing [Shamberger and Garcia, 2007]. This deeper reservoir is linked to the summit reservoir by a dike emplaced at the start of the eruption [e.g., Cervelli and Mikus, 2003].

3. Methods

[7] The thermal evolution of the shallow Pu'u 'Ō'Ō magma reservoir is modeled as the cooling of an infinite two-dimensional dike-like body (see Figure 4). The standard heat equation is solved, allowing for spatially variable thermal conductivity, K , and the inclusion of the latent heat of fusion, L ,

$$\rho c_p \frac{\partial T}{\partial t} = \nabla \cdot (K \nabla T) + L(T) \rho \cdot \frac{\partial M_{\text{stal}}}{\partial t} \quad (1)$$

where ρ is the magma density (assumed constant), c_p is the heat capacity, dt is the time step and M_{stal} is the mass fraction crystallized. Equation (1) is

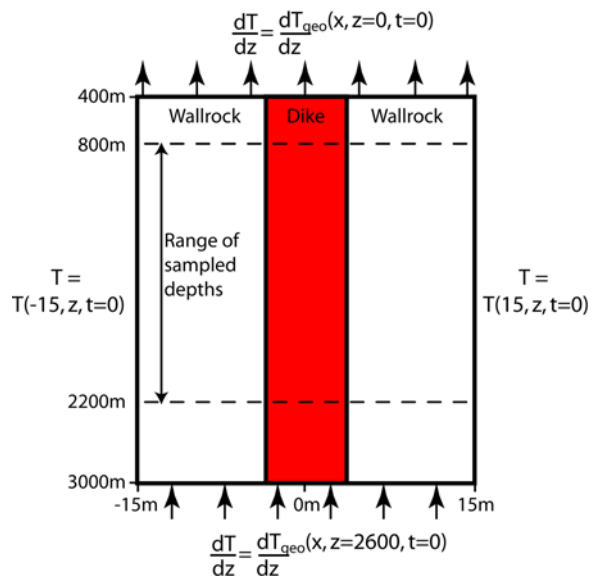


Figure 5. The boundary conditions for the model include constant temperature vertical boundaries with fixed flux top and bottom boundaries. The boundaries are far from the region of interest in this study (within the dashed lines, close to the dike) and have little effect on the final temperatures within the model.

Table 1. Model Parameters

Parameter	Description	Value	Units
K	thermal conductivity	2.7–17	$\text{W m}^{-1} \text{K}^{-1}$
ρ	density	2700	Kg m^{-3}
c_p	heat capacity	1000	$\text{J kg}^{-1} \text{ } ^\circ\text{C}^{-1}$
T_o	initial dike temperature	1245	$^\circ\text{C}$
t_{res}	residence time	31	days
t_{init}	time of prior magma storage	2	years
dT_{geo}/dz	geothermal gradient	40–250	$^\circ\text{C km}^{-1}$
Z_o	initial depth of simulation	400	m
L	latent heat	325–440	kJ kg^{-1}
Δd	grid spacing	0.25	m

discretized using a standard Eulerian finite difference method with forward differencing in time that is first-order accurate and central differencing in space that is second-order accurate. Calculations are performed in cross-section on a two-dimensional (2-D) grid with spacing of 0.25 meters to enable resolution of the thermal evolution within the dike and a time step equal to a hundredth of the diffusion timescale. A decrease in the grid spacing by 20% produces a change in the final temperature of less than $\sim 1\%$. The model domain is 2600 meters in height (depths from 400 to 3000 meters) and 30 meters wide. The simulated dike is placed at the center of this domain and is of equal height and 3.5 meters in width on the basis of modeling of reservoir deformation [Hoffmann *et al.*, 1990]. A heat flux condition, equal to the geothermal gradient, based on well data from Kīlauea's east rift zone [Bargar *et al.*, 1995], is imposed upon the top and bottom boundaries (Figure 5). Excess heat loss from the top of the dike by magma degassing is probably minor because the top of the dike (400 m) is deeper than the likely maximum degassing depth for rift zone magmas (~ 300 m [Moore, 1970]). The vertical boundaries are at a constant temperature based upon the initial condition (see below). The constant temperature conditions do not impact the solution within the dike boundaries as the distance between the dike wall and the domain boundary (13.25 m) is nearly an order of magnitude larger than the characteristic diffusion length scale (1.65 m) for the duration of time considered here. Additionally, the constant heat flux conditions on the top and bottom boundaries are >200 meters from the region of interest within the model and do not strongly effect the solution (Figure 5). Other model parameter values are given in Table 1.

[8] The continuous presence of magma in the shallow Pu`u`O`o reservoir since episode 1 [Wolfe *et al.*, 1987; Heliker and Mattox, 2003] provides a

constraint on the initial thermal condition of the surrounding wall rock. The initial temperature field outside of the dike boundaries, T_{init} , is assumed to be that of a material with variable thermal conductivity of uniform temperature in contact with an isothermal boundary of temperature equal to the magma temperature, T_{magma} , for 2 years, the time between the eruption of episode 1 to the end of episode 29, t_{init} ,

$$T_{init}(x, z) = T_{geo}(z) + (T_{magma} - T_{geo}(z)) \cdot \text{erfc}\left(\frac{x}{2\sqrt{\kappa(z)t_{init}}}\right), \quad (2)$$

where z is depth in the model, x is horizontal distance from the dike wall and κ is the thermal diffusivity [Turcotte and Schubert, 2002]. The geotherm of the host rock, T_{geo} , is based upon the temperature profiles at the SOH 1, 2 and 4 drill holes along the east rift zone of Kīlauea (Figure 1) [Bargar *et al.*, 1995]. This temperature profile implies temperatures above the liquidus for a small region of wall rock at the edge of the reservoir. This is not observed in the Pu`u`O`o lavas [Garcia *et al.*, 1992] and this region rapidly cools below the liquidus as the model evolves. Each drill hole shows an initial temperature of $\sim 35^\circ\text{C}$ at ~ 400 meters (depth to top of reservoir) with a geothermal gradient between 40 and $100^\circ\text{C}/\text{km}$ at depths less than ~ 1000 – 1400 meters followed by a sharp increase in the gradient over a few hundred meters to ~ 230 – $270^\circ\text{C}/\text{km}$. We set the deep model thermal gradient to the average of these values ($250^\circ\text{C}/\text{km}$) and examine the full range of shallow values.

[9] Utilizing the observed change in thermal gradient, we impose a depth variation in the thermal conductivity of the country rock. In an ideal box at thermal steady state with a fixed basal heat flux,

Table 2. Initial Episode 30 Magma Composition Used in MELTS Modeling^a

SiO ₂	TiO ₂	Al ₂ O ₃	Fe ₂ O ₃	FeO	MnO	MgO	CaO	Na ₂ O	K ₂ O	P ₂ O ₅	H ₂ O
50.02	2.37	12.69	1.84	9.52	0.17	9.48	10.72	2.21	0.45	0.23	0.30

^aBased upon analysis of sample 30–362 [Garcia *et al.*, 1992] with 0.30 wt% H₂O added and normalized to 100%.

the thermal conductivity controls the thermal gradient. Assuming a heat flux of 0.68 W m⁻² (K = 2.7 W m⁻¹ C⁻¹, dT_{geo}/dz = 250°C/km) at the base of the ideal box, the calculated range of shallow conductivities for geothermal gradients between 40°C/km and 100°C/km is 7 to 17 W m⁻¹ C⁻¹. Using this calculation, the model wall rock temperature begins at 35°C and is subject to a shallow thermal gradient between 40°C/km and 100°C/km up to a depth of 1650 meters. A short transition zone (~300 meters) is followed by a steep thermal gradient of 250°C/km below 1950 meters depth. The thermal conductivity within the dike is constant and equal to the deep thermal conductivity (2.7 W m⁻¹ C⁻¹).

[10] The latent heat of fusion and the rate of crystallization is calculated utilizing the MELTS algorithm [Ghiorso and Sack, 1995]. The initial magma composition (Table 2) for the MELTS calculations is based on the lava composition at the end of episode 30, which is considered a parental magma composition for this portion of the eruption [Garcia *et al.*, 1992], with 0.3 wt% H₂O added on the basis of previous studies of Kīlauea lavas [Byers *et al.*, 1985]. The pressure was set at 500 bars and the oxygen fugacity buffer at QFM, with the buffer unconstrained during cooling. After finding the liquidus temperature (1230°C), the magma was cooled in 2°C steps. The phenocryst assemblages calculated by MELTS accurately reproduce those found in Pu'ū 'Ō'Ō lavas [Garcia *et al.*, 1992]. The latent heat and the percent of crystallization are output values from the MELTS algorithm (Figure 6) and are implemented in our model calculations through $L(T)$ and M_{xtal} (equation (1)).

[11] We convert depth in our model to the time of eruption by making the simplifying assumption that the reservoir erupts from the top down. The dimensions of the dike-like reservoir are assumed to be uniform with depth. Episode 30 erupted a dense rock equivalent of 9.9×10^6 m³ over a period of 21 hours [Heliker and Mattox, 2003] giving an average effusion rate of ~131 m³/s. For the dimensions of the dike (3.5 m wide, 1600 m long), the surface area (at any given depth) is

5600 m². Thus, for a constant effusion rate (no data are available to constrain effusion rate variations during episode 30), the eruption is estimated to have vertically sampled the reservoir at a rate of 0.0234 m/s.

[12] This study models the thermal evolution of magma within the shallow magma reservoir beneath Pu'ū 'Ō'Ō between the end of episode 29 and the start of episode 30. The thermal evolution of Pu'ū 'Ō'Ō magma is evaluated with the MgO thermometer for Kīlauea lavas [Helz and Thornber, 1987] using samples collected 1 to 3.5 hours apart from episode 30 (M. Garcia *et al.*, manuscript in preparation, 2007). It has been shown that crystals generally form at the walls of magma systems and are removed from the system as they are created [McBirney, 1992]. We do not simulate crystal settling. Although degassing and cooling occurs during eruption of the Pu'ū 'Ō'Ō lavas, there is little crystallization in rapidly quenched samples (microlites in a glassy matrix)

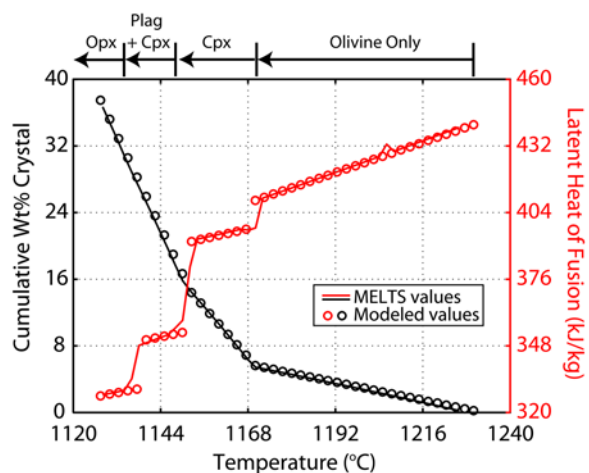


Figure 6. Variations in latent heat of fusion and cumulative crystal content (solid lines) for a cooling episode 30 initial magma (Table 2) at 500 bars based on calculations using the MELTS algorithm. Olivine is the liquidus mineral. It is followed by clinopyroxene at 1171°C and plagioclase at 1148°C. The entrance of these phases corresponds to drops in the latent heat. The resulting values are approximated for use in the model (circles).

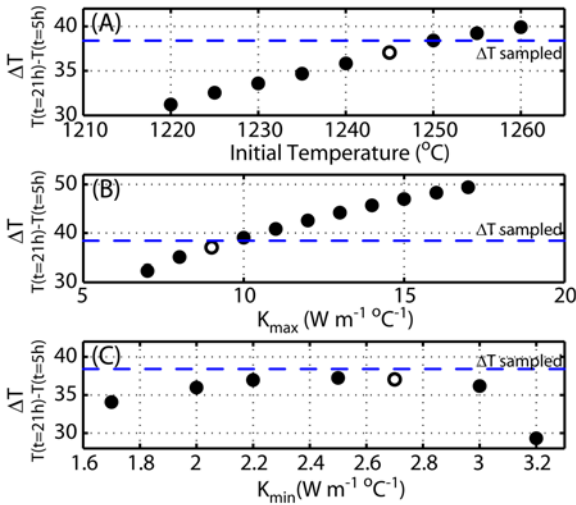


Figure 7. The temperature differences between model depths corresponding to 5 and 21 hours after the start of episode 30 are plotted versus (a) initial temperature of the magma, (b) maximum thermal conductivity of the wall rock, and (c) the minimum thermal conductivity of the wall rock (also the conductivity of the magma in the dike). The open black circles correspond to the preferred model in Figure 9. The dotted black line is the temperature difference between the initial and final sample of the Pu`u`O`o data.

[Garcia *et al.*, 1992]. Thus final model temperatures are assumed to correspond with eruption temperatures. The models are run for the equivalent of 31 days to match the magma residence time between episodes 29 and 30.

4. Model Sensitivity

[13] A range of values for initial magma temperature, maximum thermal conductivity and minimum thermal conductivity are explored to determine how sensitive the model is to changes in these parameters. Although other variables are important to the final model temperatures, these are the least constrained by other data. Figure 7 shows the parameters plotted versus the difference in temperature between the model depths corresponding to the initial and final samples from episode 30. The temperature difference illustrates the range of temperatures that each model run will span with the given set of parameter values. This shows the model is most sensitive to changes in the initial magma temperature and the maximum thermal conductivity. Changes in the minimum thermal conductivity display an upside-down parabolic shape due to the decreased difference between the minimum and maximum conductivity with

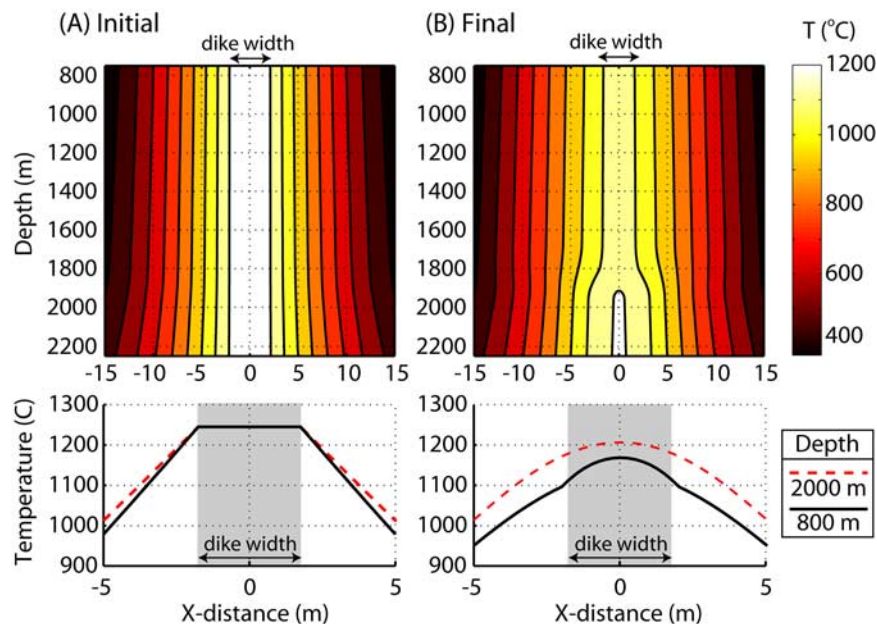


Figure 8. (a) Modeled temperature variations within the Pu`u`O`o shallow magma reservoir after the influx of a new batch of MgO-rich magma (initial) and (b) just before the start of an eruptive episode (final). The depth range shown corresponds to the eruptive times in Figure 9. Lateral temperature variations (bottom panels) at two depths (dashed line, 2000 m; solid line, 800 m) demonstrate the cooling across the dike and the effect of different thermal conductivities between the magma and the wall rock. Variation in thermal conductivity is 2.7 to 9 $\text{W m}^{-1} \text{ } ^{\circ}\text{C}^{-1}$, and the change in the geotherm is 59 $^{\circ}\text{C}/\text{km}$ to 250 $^{\circ}\text{C}/\text{km}$.

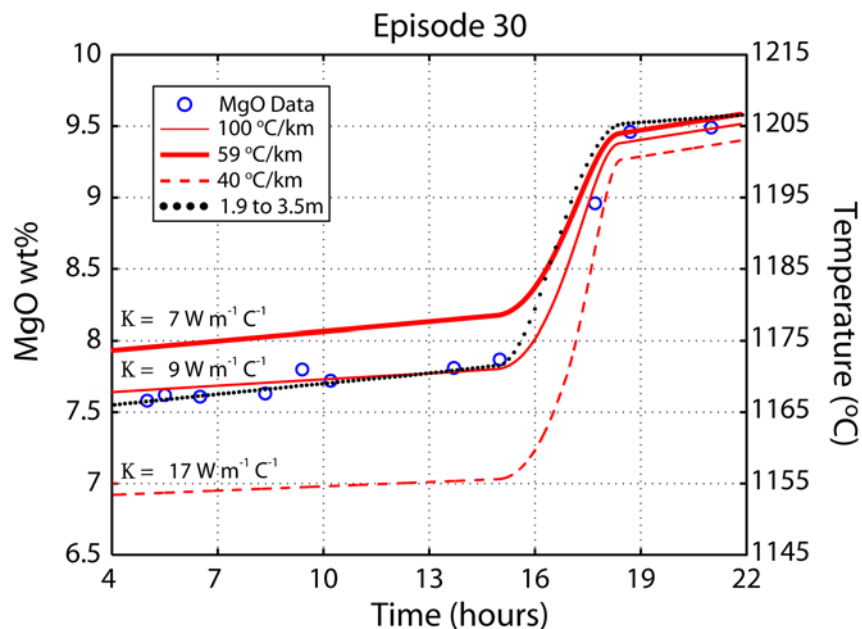


Figure 9. Temporal variation of rock MgO and temperature during episode 30 (circles) are compared to modeled temperatures (curves). Sample temperatures are based on the MgO thermometer of *Helz and Thornber* [1987]. Results are shown for shallow thermal conductivities of $7 \text{ W m}^{-1} \text{ K}^{-1}$ (thin line), $9 \text{ W m}^{-1} \text{ K}^{-1}$ (thick line), and $17 \text{ W m}^{-1} \text{ K}^{-1}$ (dashed line), which correspond to geothermal gradients of 100, 59, and $40^\circ\text{C}/\text{km}$, respectively, which are within the range of values observed for Kīlauea’s east rift zone [*Bargar et al.*, 1995]. Additionally, variation in dike width from 1.9 to 3.5 m (dotted line) will reproduce a similar pattern of temperature variations.

the increasing minimum value, although this variation is small.

5. Results and Discussion

[14] *Latypov* [2003] speculated that chemical variation in some magma bodies may be controlled solely by wall rock thermal gradients, but did not quantitatively evaluate this hypothesis. We explore quantitatively the effects of wall rock thermal gradients on magma reservoir crystallization to constrain the conditions necessary to produce a sharp compositional boundary in the Pu`u`O`o magma reservoir. The heat equation is solved with variable thermal conductivity in space and the addition of the latent heat of fusion. On the basis of thermal gradients in drill holes along Kīlauea’s east rift zone, the geothermal gradient is assumed to be $250^\circ\text{C}/\text{km}$ below 1950 m (eruption times >18.4 hours), and $40^\circ\text{C}/\text{km}$ to $100^\circ\text{C}/\text{km}$ for depths shallower than 1650 m (eruption time <14.5 hours), with an intervening transition zone.

5.1. Pu`u`O`o Eruption, Episode 30

[15] Final thermal gradients and temperatures in the magma reservoir are primarily controlled by the

thermal conductivity and geothermal gradient of the surrounding country rock (Figure 8). The thermal conductivity of $2.7 \text{ W m}^{-1} \text{ C}^{-1}$ (equivalent to a thermal diffusivity $\sim 1 \times 10^{-6} \text{ m}^2 \text{ s}^{-1}$ of olivine for temperatures above $\sim 250^\circ\text{C}$ [*Clauser and Huenges*, 1995]) chosen for eruption times after 18.4 hours (depths > 1950 m) leads to a temperature at the center of the dike at the time (depth) of the final sample (21 hours after the eruption started, at a depth of 2170 m) of $\sim 1205^\circ\text{C}$. The temperatures at the center of the dike at the time (depth) of the initial sample (4.3 hours, 762 m) range from 1153°C to 1174°C depending upon the shallow thermal conductivity (7 to $17 \text{ W m}^{-1} \text{ C}^{-1}$). The compositional variation for episode 30 can be reproduced, with a minimum in the root-mean square (RMS) misfit between the modeled and sampled temperature values (Figure 10), using an initial magma temperature of 1245°C (slightly higher than calculated liquidus) and a thermal conductivity that varies from $2.7 \text{ W m}^{-1} \text{ C}^{-1}$ to $9 \text{ W m}^{-1} \text{ C}^{-1}$ (Figures 9 and 10). Although this temperature is slightly above the liquidus temperature, it is well below the maximum calculated magma temperature (1320°C) from the measured MgO at borehole SOH1 [*Quane et al.*, 2000]. The mechanism that produces this change in thermal conductivity may

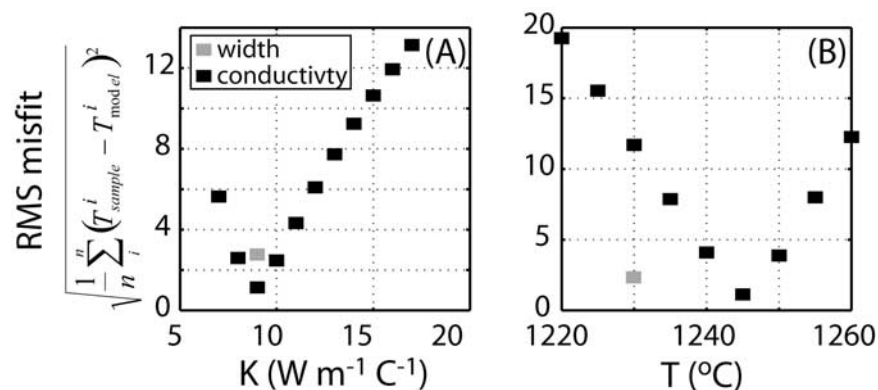


Figure 10. The root mean square (rms) values of the misfit between the Pu`u`Ō`Ō data and the model for (a) a range of maximum thermal conductivities and (b) a range of starting magma temperatures with a maximum thermal conductivity of $9 \text{ W m}^{-1} \text{ C}^{-1}$. The value for the changing width model (gray boxes) is slightly higher than the best three fits for the model with changing thermal conductivity. All the sampled values from episode 30 are incorporated in the RMS calculation ($n = 11$, number of samples).

be related to hydrothermal cooling, dike injection or both, as described below. Regardless of the mechanism, it must be capable of producing a sharp change in thermal properties over a short distance ($\sim 300 \text{ m}$).

[16] Hydrothermal cooling associated with subsurface water suggested to be present along the East Rift Zone [Bargar *et al.*, 1995] may act to change the geothermal gradient, but could be limited to shallow depths. The observed change in the geothermal gradient with depth in Kīlauea's east rift zone correlates with a dramatic increase in dike abundance in the SOH1 drill core below $\sim 1200 \text{ m}$ [Quane *et al.*, 2000]. Dikes are impermeable to fluid flow and act as aquicludes in Hawaiian volcanoes [e.g., Macdonald *et al.*, 1983]. Additionally, fluid flow is impaired at depth within lava sequences by the lower permeability resulting from the growth of secondary minerals (clays and zeolite [Keller *et al.*, 1979; Schiffman *et al.*, 2006]).

[17] An alternative explanation for the thermal gradients in the shallow reservoir includes a sharp increase in reservoir thickness, assuming the geothermal gradient and thermal conductivity are constant. For example, the thermal evolution of a dike that changes width from 1.9 to 3.5 m between 1650 and 1950 meters, a thermal conductivity of $2.7 \text{ W m}^{-1} \text{ C}^{-1}$ and a geothermal gradient of $115^\circ\text{C}/\text{km}$, successfully reproduces the MgO variation seen in the data (Figure 9, dotted line) with an RMS misfit similar to the best model with varying thermal conductivity. The width of an intruding dike is largely controlled by the stiffness of the surrounding wall rock (assuming constant driving pressure in the dike). In the case of Pu`u`Ō`Ō, this

would suggest a decrease in stiffness with depth. One way to decrease stiffness is through the introduction of voids that may act on the rock like a reduction of the Young's modulus [Lemaitre, 1992]. The SOH1 stratigraphic section shows the opposite trend as the abundance of pahoehoe and a'a lavas (greater void spaces) decreases in favor of dike intrusions and massive basalt at depth (i.e., less stiff to more stiff) [Quane *et al.*, 2000]. The current models of reservoir deformation do not simulate a dike of changing thickness [Okamura *et al.*, 1988; Hoffmann *et al.*, 1990]. Thus this model cannot be independently evaluated.

[18] The above models assume that the temperature at the center of the dike is representative of the erupted temperatures. Lateral variation of the temperature across the model dike is 1–2 times the vertical temperature variation (Figure 8). Across dike temperature variation should produce rapid and large MgO variation within the erupted lavas. This is not observed in the episode 30 lavas (Figure 2) (M. Garcia *et al.*, manuscript in preparation, 2007). Thus some form of small scale mixing is probably necessary to minimize lateral thermal gradients within the reservoir.

[19] Lateral density variations are inherently unstable and will induce convective motion within the cooling reservoir. In order to justify a conductive cooling solution for the temperatures within the dike, these motions must be small relative to the height of the reservoir. Stevenson and Blake [1998] estimate terminal rise velocities of dense, degassed magma within vertical conduits. Using their empirical law for Poiseuille number and a parameterization of terminal rise velocity, we calculate the

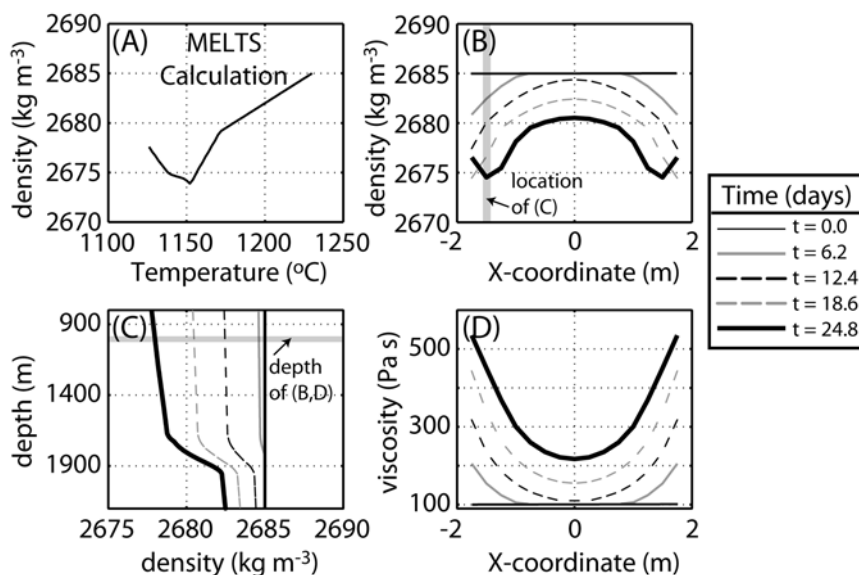


Figure 11. The temperature calculations from the preferred model at 5 time steps combined with (a) the MELTS calculations allow the examination of density variations (b) across the dike at 1000 m depth and (c) with depth 0.25 m from the left edge of the dike. MELTS also calculates the viscosity of the magma which is (d) plotted at 1000 m depth. Both viscosity and density are of the liquid phase as the crystals are assumed to adhere to the walls of the reservoir as they are formed.

distance traveled by a mass of uniform viscosity and uniform density fluid 0.25 m across and 0.25 m from the reservoir edge with a viscosity and density contrast measured between the conduit location and the reservoir center. Calculating this value at 5 different times throughout the model run (Figure 11), we find that [Stevenson and Blake, 1998, equations (1) and (11)] magma at 1000 m depth should travel approximately 172 m (<10% of the reservoir height). However, as magma descends (ascends) it will enter regions of warmer (cooler) temperature and more (less) dense material which will act to oppose this motion. As cooling proceeds, the magma decreases somewhat in density (10 kg m^{-3}) during olivine-only and clinopyroxene crystallization, and then the trend reverses as plagioclase crystallizes (Figure 11a). This density variation will tend to increase and then decrease positive buoyancy. These factors suggest that 172 meters is probably an upper bound to the motion experienced in the reservoir. Additionally, there is a large increase in density with depth corresponding to the large decrease in thermal conductivity in the wall rock and thus motion across this boundary is unlikely.

5.2. Other Episodes

[20] Temporal MgO variation is also seen in episodes 5–10 and 31 of the current Pu`u`O`o eruption (Figure 3). Most of the MgO variation

during episode 31 (7.7 to 8.9 wt%) occurred over <3 hours [Garcia *et al.*, 1992]. During episodes 5–10, the lava compositions show a mean variation of 1.35 wt% MgO with a standard deviation of 0.36 wt%. Episode 7 was the best sampled (5) of these episodes; it shows an MgO increase from 6.8–7.85 wt% during the 56 hour eruption, with a change from 7.0–7.6 wt% during a 14 hour period (Figure 2). The lack of detailed sampling of this and other early episodes with significant compositional variation prevent us from making a more detailed comparison with episode 30. However, all these episodes show the same trend from lower MgO at the beginning followed by higher MgO (Figure 3), supporting the overall features addressed in the modeling.

[21] Other Pu`u`O`o episodes show little or no compositional variation [Garcia *et al.*, 1992]. The lack of variation may be related to the percent of the magma reservoir that was erupted. If an episode tapped only the upper region of the shallow reservoir, then our model predicts that the higher MgO lavas would not be observed. Episodes 30 and 31 erupted relatively large volumes of magma (9.9 and 13.6 Mm^3 [Heliker and Mattox, 2003]), nearly or possibly completely emptying the 10 – 12 Mm^3 magma reservoir [Hoffmann *et al.*, 1990] allowing fresh, uniform temperature, high MgO magma to fill the reservoir. Between episode 10 and episode 29 only one episode (18) erupted greater than 75%

of the estimated reservoir size [Heliker and Mattox, 2003]. Approximately 16.8 Mm^3 of lava were erupted in episode 18, although the lava is uniform in MgO (7.5 wt% [Garcia et al., 1992; Heliker and Mattox, 2003]). The lack of compositional variability in episode 18 lavas may be related to relatively small volumes that were erupted during episodes 11–17 ($4.2\text{--}8.4 \text{ Mm}^3$ [Heliker and Mattox, 2003]), which probably did not flush out the magma reservoir allowing accumulation of cooler, lower MgO magma. After episode 31, there were three episodes that erupted $>10 \text{ Mm}^3$, prior to a switch in eruptive style to continuous effusion during episode 48 [Heliker and Mattox, 2003]. However, these episodes showed essentially no compositional variation [Garcia et al., 1992]. The lack of compositional variation during episodes 37 and 38 also may be related to incomplete flushing of the reservoir during episodes 33–36 ($5.5\text{--}8.4 \text{ Mm}^3$). Episode 32 does not display compositional variation and erupts a large volume of magma (11.4 Mm^3), but documentation of other potential influences (such as inflation during the repose period) are poorly documented for this episode [Hoffmann et al., 1990].

5.3. Chemical Interfaces in Other Magma Bodies

[22] Other historical eruptions have also shown relatively sharp compositional changes that reflect a zoned magma chamber. Crystal fractionation is thought to have the dominant role in generating much of the compositional variation in these examples, although crustal assimilation was also important in many continental eruptions (e.g., Paricutin [Wilcox, 1954; McBirney et al., 1987], Jorulla [Luhr and Carmichael, 1985]). Some eruptions have produced the same trend from lower to higher MgO as displayed during the Pu' u 'Ō' ō episodic eruptions (e.g., 1968 to present, Arenal volcano in Costa Rica [Reagan et al., 1987]; 1759–1774 Jorullo Volcano in Mexico [Luhr and Carmichael, 1985]), whereas others have displayed a reverse trend (e.g., Sept. 1982 Kīlauea summit eruption [Garcia et al., 2003]; 1943–1951 Paricutin eruption in Mexico [Wilcox, 1954]). Most of these eruptions were not densely sampled, so the details of the compositional variation are poorly known. An exception is the Sept. 1982 Kīlauea eruption, with seven samples from the vent areas during a ~ 14 hour period. Analyses of these samples show that the lava varied from 8.5 to 6.8 wt.% MgO over <10 hours. This reverse trend may reflect tapping the base or flanks of a zoned magma

chamber [Garcia et al., 2003]. The geometry of the Kīlauea summit reservoir is unknown; models vary from a plexus of dikes and sills [Tilling and Dvorak, 1993] to a $1\text{--}2 \text{ km}^3$ spherical reservoir [Pietruszka and Garcia, 1999]. Whatever the shape, it is clear that the sharp compositional zonation observed during the early Pu' u 'Ō' ō episodes is not unique and may form in reservoirs with other shapes and in different tectonic settings.

6. Conclusions

[23] Compositional variation of lavas erupted from the Pu' u 'Ō' ō vent provide valuable information about the thermal evolution of magmas within its shallow magma reservoir. The ~ 2 wt% variation in MgO during <4 hours for the 21 hour episode 30 suggests the presence of a sharp compositional boundary within the shallow magma reservoir. Through use of a simple thermal model and MgO thermometry, we find that this variation can be explained in two ways: 1. depth variation of thermal conductivity in the wall rock surrounding the uniform width reservoir, and 2. a change in reservoir width for wall rock with constant thermal conductivity. Geothermal wells in Kīlauea's east rift zone, where Pu' u 'Ō' ō is located, show a sharp change in thermal gradient with depth [Bargar et al., 1995], consistent with changing thermal conductivity. A change in dike width requires decreasing stiffness with depth which is inconsistent with drill core data for the rift zone.

[24] For the model with variable thermal conductivity, the compositional variation of the erupted lavas requires the wall rock thermal conductivity to increase from $2.7 \text{ W m}^{-1} \text{ C}^{-1}$ at depths greater than $\sim 1950 \text{ m}$ to $\sim 9 \text{ W m}^{-1} \text{ C}^{-1}$ at depths shallower than ~ 1650 meters. Results indicate that the final temperatures at the center of the dike-like reservoir are a function of the conductivity and the wall rock thermal gradient. These results indicate that wall rock temperature gradients and thermal conductivity strongly affect the chemical evolution of magma reservoirs.

Acknowledgments

[25] The authors would like to thank the current and former staff of the Hawaiian Volcano Observatory, especially Ed Wolfe and George Ulrich for access to samples they collected and for discussions on the Pu' u 'Ō' ō eruption, Bill Rose and his students for collecting the episode 30 tephra samples, Don Thomas for insights into the thermal and groundwater aspects of Kīlauea's east rift zone, Julia Hammer and Mark Ghorso

for their assistance with MELTS, Matthias Hort for discussions on our model, and Steve Martel for discussions on dike intrusion and rock compliance. We would also like to thank an anonymous reviewer, journal reviewer Taber Hersum, and editor Vincent Salters for their comments on this paper. This project was supported by NSF grant EAR03-36874 to M.G. This is SOEST contribution 7112.

References

- Bargar, K. E., T. E. C. Keith, and F. A. Trudell (1995), Fluid-inclusion evidence for past temperature fluctuations in the Kilauea east rift zone geothermal area, Hawaii, *Geothermics*, *24*, 639–659.
- Byers, C. D., M. O. Garcia, and D. W. Muenow (1985), Volatiles in pillow rim glasses from Loihi and Kilauea volcanoes, Hawaii, *Geochim. Cosmochim. Acta*, *49*, 1887–1896.
- Cayol, V., J. H. Dieterich, A. T. Okamura, and A. Miklius (2000), High magma storage rates before the 1983 eruption of Kilauea, Hawai'i, *Science*, *288*, 2343–2346.
- Cervelli, P. F., and A. Miklius (2003), The shallow magmatic system of Kilauea Volcano, *U.S. Geol. Surv. Prof. Pap.*, *1676*, 149–163.
- Clauser, C., and E. Huenges (1995), Thermal conductivity of rocks and minerals, in *Rock Physics and Phase Relations: A Handbook of Physical Relations, AGU Ref. Shelf Ser.*, vol. 3, edited by T. J. Ahrens, pp. 105–126, AGU, Washington, D. C.
- Dzurisin, D., R. Y. Koyanagi, and T. T. English (1984), Magma supply and storage at Kilauea Volcano, Hawai'i 1956–1983, *J. Volcanol. Geotherm. Res.*, *21*, 177–206.
- Garcia, M. O., and E. W. Wolfe (1988), Petrology of the lavas from the Pu'u 'Ō'ō eruption of Kilauea Volcano, Hawaii: Phases 1–20, *U.S. Geol. Surv. Prof. Pap.*, *1463*, 127–143.
- Garcia, M. O., R. A. Ho, J. M. Rhodes, and E. W. Wolfe (1989), Petrologic constraints on rift-zone processes: Results from episode 1 of the Pu'u 'Ō'ō eruption of Kilauea Volcano, Hawai'i, *Bull. Volcanol.*, *52*, 81–96.
- Garcia, M. O., J. M. Rhodes, E. W. Wolfe, G. E. Ulrich, and R. A. Ho (1992), Petrology of lavas from episodes 2–47 of the Pu'u 'Ō'ō eruption of Kilauea Volcano, Hawai'i: Evaluation of magmatic processes, *Bull. Volcanol.*, *55*, 1–16.
- Garcia, M. O., A. J. Pietruszka, and J. M. Rhodes (2003), A petrologic perspective of the summit magma chamber of Kilauea Volcano, Hawaii, *J. Petrol.*, *44*, 2313–2339.
- Ghiorso, M. S., and R. O. Sack (1995), Chemical mass-transfer in magmatic processes 4: A revised and internally consistent thermodynamic model for the interpolation and extrapolation of liquid-solid equilibria in magmatic systems at elevated temperatures and pressures, *Contrib. Mineral. Petrol.*, *119*, 197–212.
- Heliker, C. C., and T. N. Mattox (2003), The first two decades of the Puu Oo-Kupaianaha eruption: Chronology and selected bibliography, *U.S. Geol. Surv. Prof. Pap.*, *1676*, 1–28.
- Helz, R. T., and C. R. Thornber (1987), Geothermometry of Kilauea Iki lava lake, *Bull. Volcanol.*, *49*, 651–658.
- Hoffmann, J. P., G. E. Ulrich, and M. O. Garcia (1990), Horizontal ground deformation patterns and magma storage during the Pu'u 'Ō'ō eruption of Kilauea Volcano, Hawai'i: Episodes 22–42, *Bull. Volcanol.*, *52*, 522–531.
- Keller, G. V., L. T. Grose, J. C. Murray, and C. K. Skokan (1979), Results of an experimental drill hole at the summit of Kilauea Volcano, Hawaii, *J. Volcanol. Geotherm. Res.*, *5*, 345–385.
- Klein, F. W., R. Y. Koyanagi, J. S. Nakata, and W. R. Tanigawa (1987), The seismicity of Kilauea's magma system, *U.S. Geol. Surv. Prof. Pap.*, *1350*, 1019–1185.
- Koyaguchi, T. (1989), Chemical gradients at diffusive interfaces in magma chambers, *Contrib. Mineral. Petrol.*, *103*, 143–152.
- Kuritani, T., T. Yokoyama, K. Kobayashi, and E. Nakamura (2003), Shift and rotation of composition trends by magma mixing: 1983 eruption of Miyake-jima Volcano, *J. Petrol.*, *44*, 1895–1916.
- Latypov, R. M. (2003), The origin of basic-ultrabasic sills with S-, D-, and I-shaped compositional profiles by in situ crystallization of a single input of phenocryst-poor parental magma, *J. Petrol.*, *44*, 1619–1656.
- Lemaitre, J. (1992), *A Course on Damage Mechanics*, 210 pp., Springer, New York.
- Luhr, J. F., and I. S. E. Carmichael (1985), Jorullo Volcano, Michoacan, Mexico (1759–1774): The earliest stages of fractionation in calc-alkaline magmas, *Contrib. Mineral. Petrol.*, *90*, 142–161.
- Macdonald, G. A., A. T. Abbott, and F. L. Peterson (1983), *Volcanoes in the Sea: The Geology of Hawaii*, 517 pp., Univ. of Hawai'i Press, Honolulu.
- McBirney, A. R. (1992), Volcanology, in *Techniques for Determining Probabilities of Geologic Events and Processes*, edited by R. L. Hunter and C. J. Mann, pp. 167–184, Oxford Univ. Press, New York.
- McBirney, A. R., H. P. Taylor Jr., and R. L. Armstrong (1987), Paricutin revisited: A classic example of crustal assimilation in calc-alkaline magma, *Contrib. Mineral. Petrol.*, *95*, 4–20.
- Moore, J. G. (1970), Water content of basalt erupted on the ocean floor, *Contrib. Mineral. Petrol.*, *28*, 272–279.
- Okamura, A. T., J. J. Dvorak, R. Y. Koyanagi, and W. R. Tanigawa (1988), Surface deformation associated with the 1983 Kilauea eruption, *U.S. Geol. Surv. Prof. Pap.*, *1463*, 165–181.
- Okubo, P. G., H. M. Benz, and B. A. Chouet (1997), Imaging the crustal magma sources beneath Mauna Loa and Kilauea volcanoes, Hawaii, *Geology*, *25*, 867–870.
- Parfitt, E. A., and L. Wilson (1994), The 1983–86 Pu'u 'Ō'ō eruption of Kilauea Volcano, Hawaii: A study of dike geometry and eruption mechanisms for a long-lived eruption, *J. Volcanol. Geotherm. Res.*, *59*, 179–205.
- Pietruszka, A. J., and M. O. Garcia (1999), The size and shape of Kilauea Volcano's summit magma storage reservoir: A geochemical probe, *Earth Planet. Sci. Lett.*, *167*, 311–320.
- Quane, S. L., M. O. Garcia, H. Guillou, and T. P. Hulsebosch (2000), Magmatic history of the East Rift Zone of Kilauea Volcano, Hawaii based on drill hole core from SOH 1, *J. Volcanol. Geotherm. Res.*, *102*, 319–338.
- Reagan, M. K., J. B. Gill, E. Malavssi, and M. O. Garcia (1987), Changes in magma composition at Arenal Volcano, Costa Rica, 1968–1985: Real-time monitoring of open system differentiation, *Bull. Volcanol.*, *49*, 415–434.
- Ryan, M. P. (1988), The mechanics and three-dimensional internal structure of active magmatic systems: Kilauea Volcano, Hawai'i, *J. Geophys. Res.*, *93*, 4213–4248.
- Schiffman, P., R. J. Watters, N. Thompson, and A. W. Walton (2006), Hyaloclastites and the slope stability of Hawaiian volcanoes: Insights from the Hawaiian Scientific Drilling Project's 3-km drill core, *J. Volcanol. Geotherm. Res.*, *151*, 217–228.
- Shamberger, P. J., and M. O. Garcia (2007), Geochemical modeling of magma mixing and magma reservoir volumes during early episodes of Kilauea Volcano's Pu'u 'Ō'ō eruption, *Bull. Volcanol.*, *69*, 345–352.

- Stevenson, D. S., and S. Blake (1998), Modelling the dynamics and thermodynamics of volcanic degassing, *Bull. Volcanol.*, *60*, 307–317.
- Tilling, R. I., and J. J. Dvorak (1993), Anatomy of a basaltic volcano, *Nature*, *363*, 125–133.
- Troise, C. (2001), Stress changes associated with volcanic systems: Constraints on Kilauea rift dynamics, *J. Volcanol. Geotherm. Res.*, *109*, 191–203.
- Turcotte, D. L., and G. Schubert (2002), *Geodynamics*, 456 pp., Cambridge Univ. Press, New York.
- Vergnolle, S., and C. Jaupart (1990), Dynamics of degassing at Kilauea Volcano, Hawaii, *J. Geophys. Res.*, *95*, 2793–2809.
- Wilcox, R. E. (1954), Petrology of Paricutin Volcano, Mexico, *U.S. Geol. Surv. Bull.*, 965–C.
- Wolfe, E. W., M. O. Garcia, D. B. Jackson, R. Y. Koyanagi, C. A. Neal, and A. T. Okamura (1987), The Pu 'u 'Ō'Ō eruption of Kilauea Volcano, episodes 1 through 20, January 3, 1983, to June 8, 1984, *U.S. Geol. Surv. Prof. Pap.*, *1350*, 471–508.
- Wolfe, E. W., C. A. Neal, N. G. Banks, and T. J. Duggan (1988), Geologic observations and chronology of eruptive events, *U.S. Geol. Surv. Prof. Pap.*, *1463*, 1–98.